Supporting Information for "Optimization of an Urban Monitoring Network for Retrieving an Unknown Point Source Emission"

Hamza Kouichi[1], Pierre Ngae[1], Pramod Kumar[1], Amir-Ali Feiz[1], and Nadir Bekka[1,2]

[1]LMEE, Université d'Evry Val-d'Essonne, 40 Rue du Pelvoux 91020 Courcouronnes, France
[2]LSA, Université Saad Dahlab-Blida, 09130 Blida, Algérie

Correspondence: Pramod KUMAR (pramod.kumar@univ-evry.fr)

Contents of this file

1. The CFD model and Simulations
2. Figures S1 to S2

List of Figures

S1.1 The optimal networks of 10 sensors for all 20 trials in the MUST field experiment. The blank and filled black circles respectively represent the all (40) potential positions and the optimal positions of sensors. 4

S1.2 The optimal networks of 13 sensors for all 20 trials in the MUST field experiment. The blank and filled black circles respectively represent the all (40) potential positions and the optimal positions of sensors. 5

S2.1 Isopleths of the renormalized weight function $(w(\mathbf{x}))$ (gray colored in first and third columns) and the normalized source estimate function $(\mathbf{s}_w^n(\mathbf{x}) = \mathbf{s}_w(\mathbf{x})/\max(\mathbf{s}_w(\mathbf{x})))$ (colored in second and fourth columns) for both optimal network respectively of 10 and 13 sensors for trials 1, 2, 3, 4, & 5. The black and white filled circles respectively represent the true and estimated source locations. 6

S2.2 Isopleths of the renormalized weight function $(w(\mathbf{x}))$ (gray colored in first and third columns) and the normalized source estimate function $(\mathbf{s}_w^n(\mathbf{x}) = \mathbf{s}_w(\mathbf{x})/\max(\mathbf{s}_w(\mathbf{x})))$ (colored in second and fourth columns) for both optimal network respectively of 10 and 13 sensors for trials 6, 7, 8, 9, & 10. The black and white filled circles respectively represent the true and estimated source locations. 7

S2.3 Isopleths of the renormalized weight function $(w(\mathbf{x}))$ (gray colored in first and third columns) and the normalized source estimate function $(\mathbf{s}_w^n(\mathbf{x}) = \mathbf{s}_w(\mathbf{x})/\max(\mathbf{s}_w(\mathbf{x})))$ (colored in second and fourth columns) for both optimal network respectively of 10 and 13 sensors for trials 11, 12, 13, 14, & 15. The black and white filled circles respectively represent the true and estimated source locations. 8

S2.4 Isopleths of the renormalized weight function $(w(\mathbf{x}))$ (gray colored in first and third columns) and the normalized source estimate function $(\mathbf{s}_w^n(\mathbf{x}) = \mathbf{s}_w(\mathbf{x})/\max(\mathbf{s}_w(\mathbf{x})))$ (colored in second and fourth columns) for both optimal network respectively of 10 and 13 sensors for trials 16, 17, 18, 19, & 20. The black and white filled circles respectively represent the true and estimated source locations. 9

1 The CFD model and Simulations

A detailed description of CFD model–fluidyn-PANACHE, used in this study, was presented in Fluidyn-PANACHE (2010) and Kumar et al. (2015). The fluidyn-PANACHE solves the Reynolds Averaged Navier-Stokes (N-S) equations using the finite volume numerical techniques. These equations were solved along with the equations describing conservation of species concentration, mass, heat transfer and energy for a mixture of ideal gases. Ideal gas law is used for the thermodynamic model of mixture of gases. The Reynolds stresses are modelled using a linear eddy viscosity model (LEVM) (Ferziger and Peric, 2002). The atmospheric boundary layer (ABL) processes are built-in the CFD code with different numerical models. Dispersion of gases is modelled by solving the full conservation equations governing the transport of species concentration. The buoyancy model is used to parametrize the body force term in the N-S equations. To couple the pressure and momentum equations in the numerical computations, the Semi-Implicit Method for Pressure Linked Equations-Consistent (SIMPLEC or SIMPLE-Consistent) algorithm (Van Doormaal and Raithby, 1984) is utilized. It includes a built-in automatic 3-D mesh generator for both structures and unstructured meshes that can generate finite-volume mesh around obstacles and body-fitting the terrain undulations.

1.1 Turbulence model

Atmospheric turbulence due to shear (flow over ground or over obstacles) as well as due to thermal effects (solar heating of ground, buoyant plumes) is modelled with a two-equations prognostic $k-\epsilon$ model. The $k-\epsilon$ model is a two-equation linear eddy viscosity model and describes the mean of a turbulent flow. It solves the transport equations for turbulent kinetic energy, k and its dissipation rate, ϵ. The fluidyn-PANACHE implementation of the $k-\epsilon$ model is derived from the standard high-Reynolds number (Re) form with corrections for buoyancy and compressibility (Launder, 2004; Hanjalic, 2005). The $k-\epsilon$ model computes the length and time scales from the local turbulence characteristics. Thus, it can model the turbulent flows subjected to both mechanical shear (obstacles, terrain undulations, canopy) as well as buoyancy (stability and buoyant/heavy gas plumes).

1.2 Boundary conditions

Depending on the wind direction with respect to the domain boundary, the lateral boundaries of the domain are treated as inflow and outflow boundaries. For ground surface, a no-slip boundary condition is considered. The top boundary is treated as an outflow boundary. In order to parameterize the drag forces on solid walls, standard wall functions (Hanjalic, 2005) are used. Following inflow boundary conditions for wind, temperature, and turbulence are specified as :

- *Wind profile* : Gryning et al. (2007) wind profile in stable and neutral conditions is used. These profiles are composed of the three different length scales in surface, middle, and upper layers of the ABL, and is applicable in the entire ABL. As the Gryning et al. (2007) wind profile is not suitable for very stable atmospheric conditions, a wind profile based on a similarity function proposed by Beljaars and Holtslag (1991) is used in extreme stability conditions due to its applicability in these stability conditions (Sharan and Kumar, 2010).

- *Temperature profile* : Monin-Obukhov similarity theory based logarithmic temperature profile is used to describe its vertical variation in neutral and stable conditions.

- *Turbulence profiles* : The profiles of k and ϵ based on an approximate analytical solution of one-dimensional $k-\epsilon$ prognostic equation (Yang et al., 2009) are used for inflow boundary conditions. Coefficients in these profiles of k and ϵ are estimated based on the observations of k.

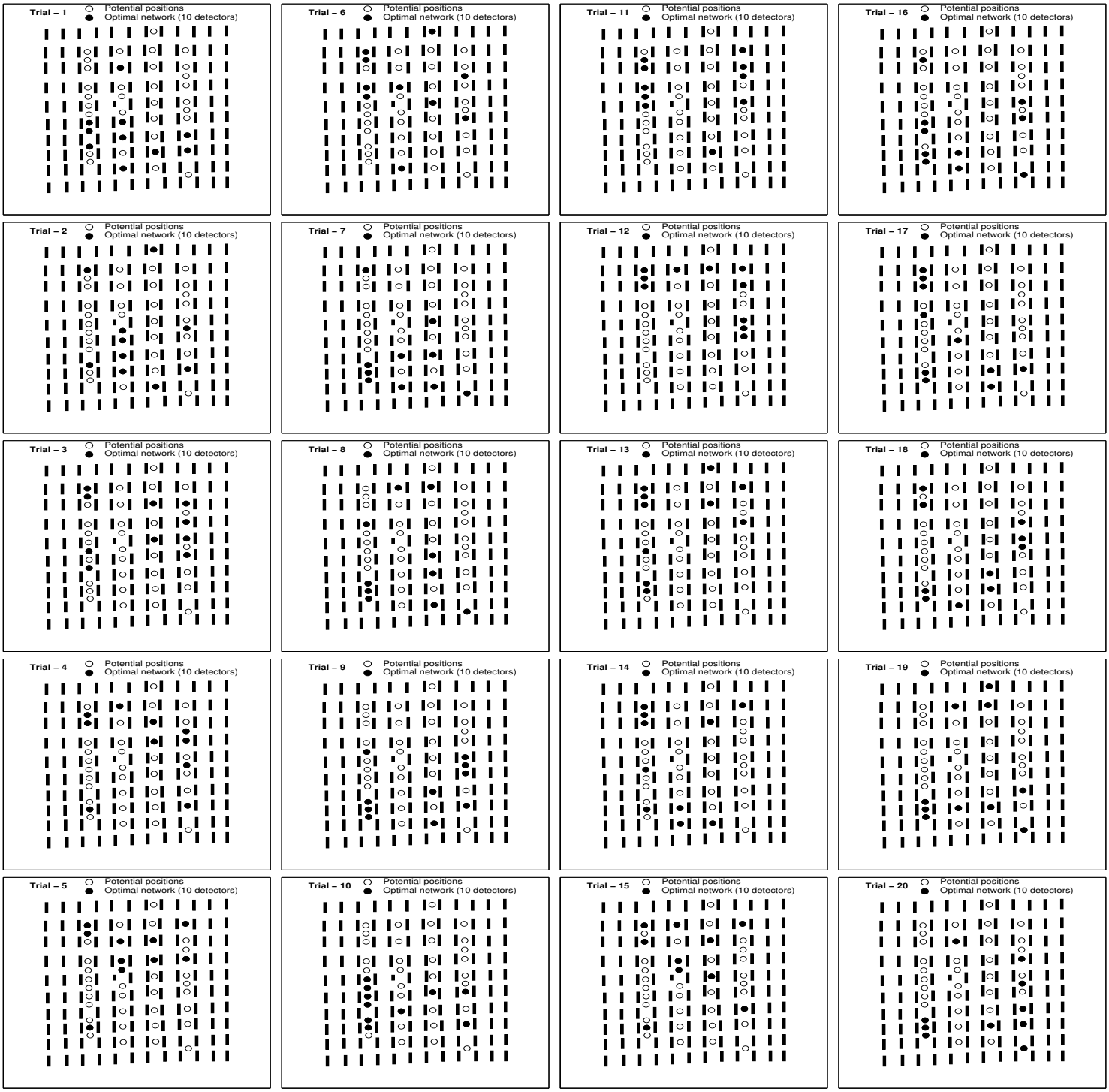

Figure S1.1. The optimal networks of 10 sensors for all 20 trials in the MUST field experiment. The blank and filled black circles respectively represent the all (40) potential positions and the optimal positions of sensors.

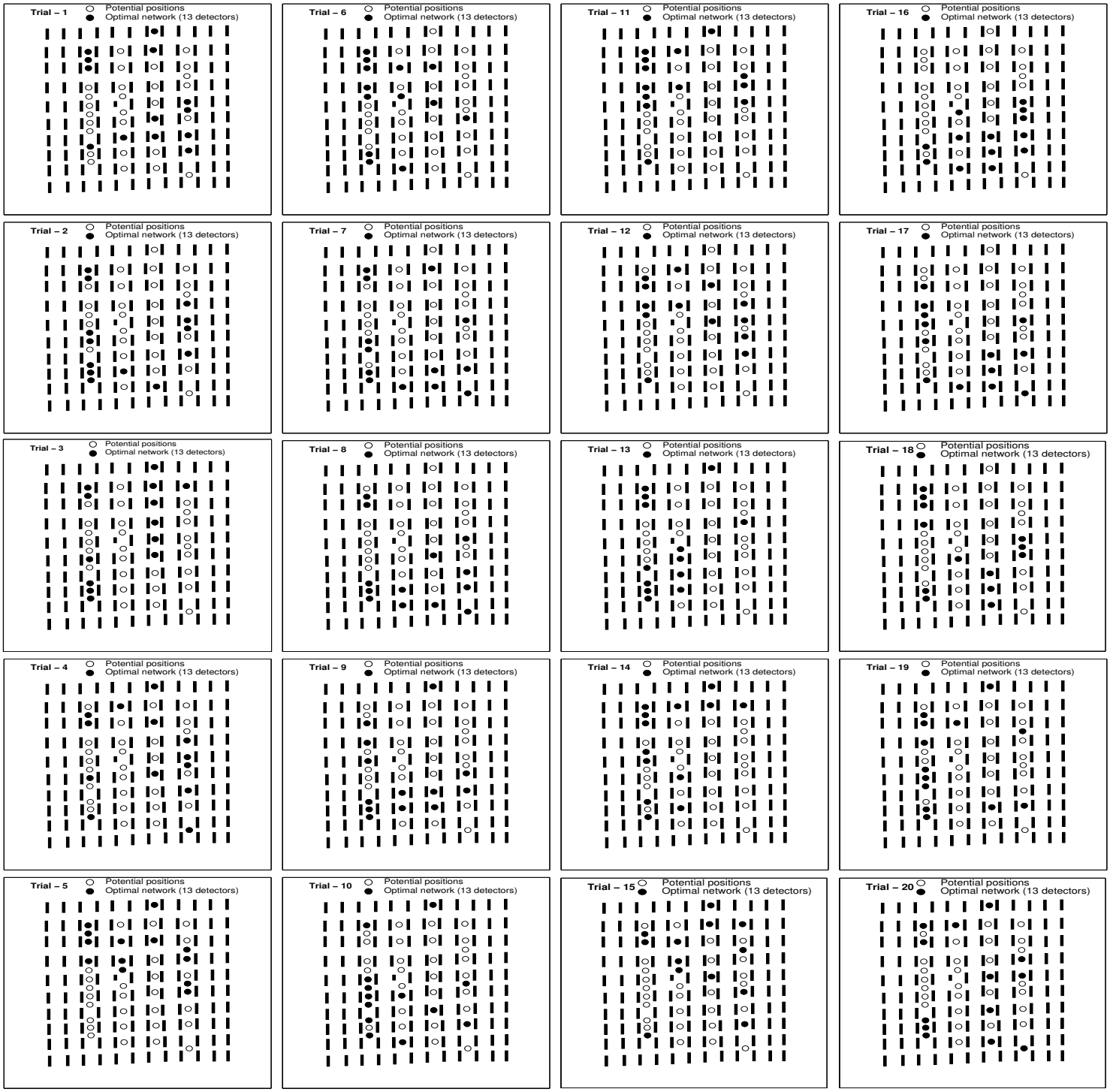

Figure S1.2. The optimal networks of 13 sensors for all 20 trials in the MUST field experiment. The blank and filled black circles respectively represent the all (40) potential positions and the optimal positions of sensors.

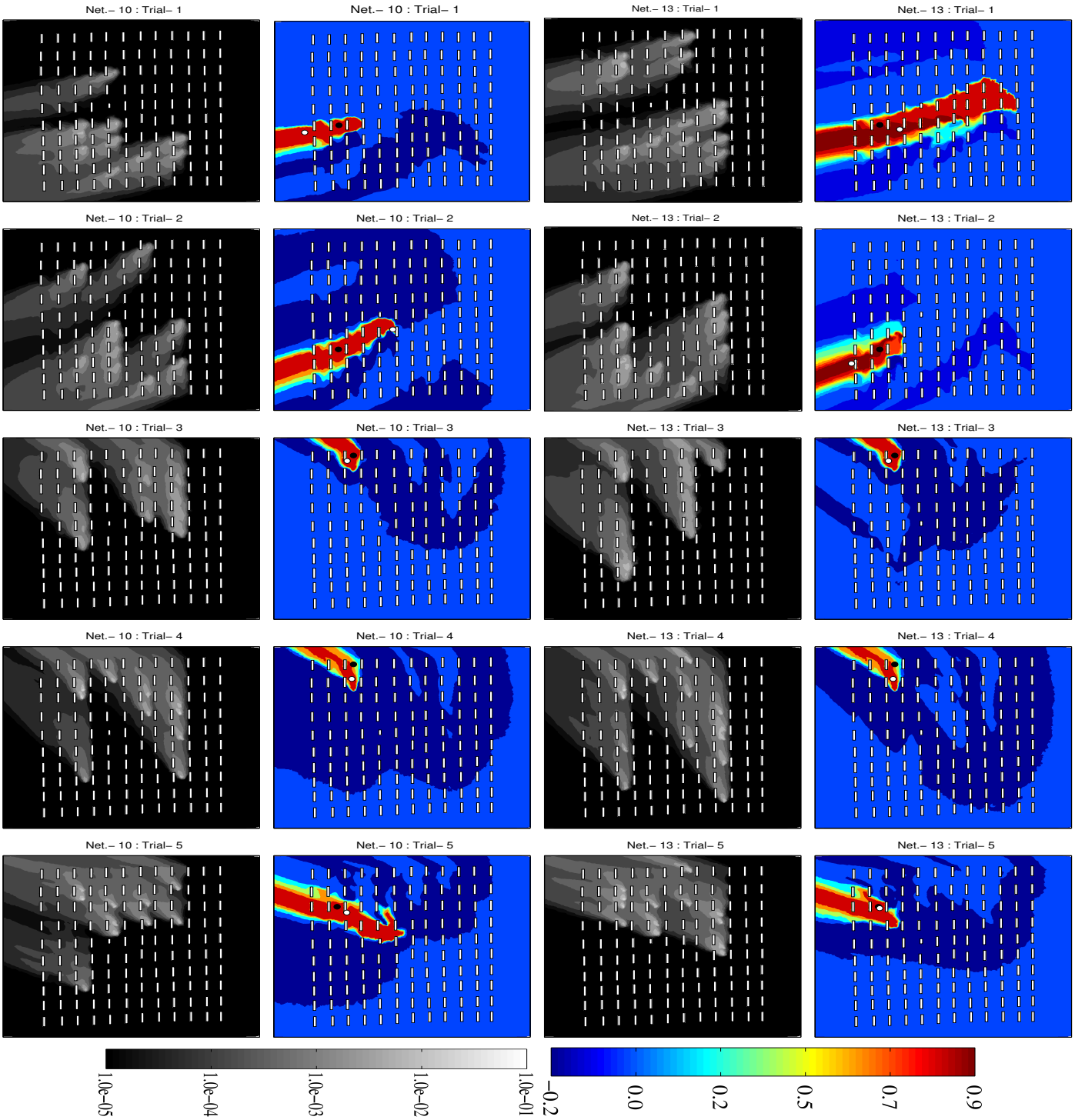

Figure S2.1. Isopleths of the renormalized weight function $(w(\mathbf{x}))$ (gray colored in first and third columns) and the normalized source estimate function $(\mathbf{s}_w^n(\mathbf{x}) = \mathbf{s}_w(\mathbf{x})/\max(\mathbf{s}_w(\mathbf{x})))$ (colored in second and fourth columns) for both optimal network respectively of 10 and 13 sensors for trials 1, 2, 3, 4, & 5. The black and white filled circles respectively represent the true and estimated source locations.

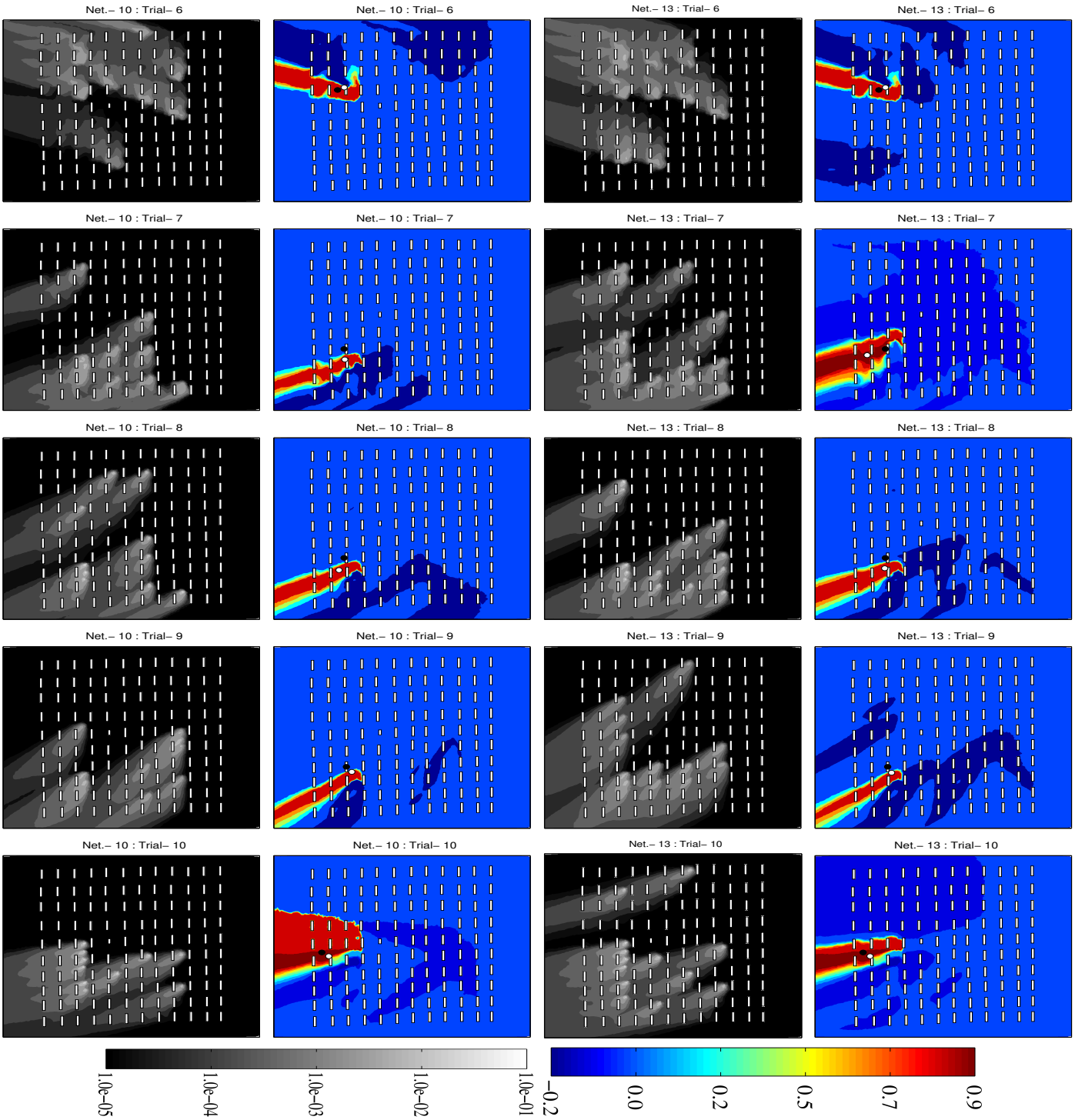

Figure S2.2. Isopleths of the renormalized weight function $(w(\mathbf{x}))$ (gray colored in first and third columns) and the normalized source estimate function $(\mathbf{s}_w^n(\mathbf{x}) = \mathbf{s}_w(\mathbf{x})/\max(\mathbf{s}_w(\mathbf{x})))$ (colored in second and fourth columns) for both optimal network respectively of 10 and 13 sensors for trials 6, 7, 8, 9, & 10. The black and white filled circles respectively represent the true and estimated source locations.

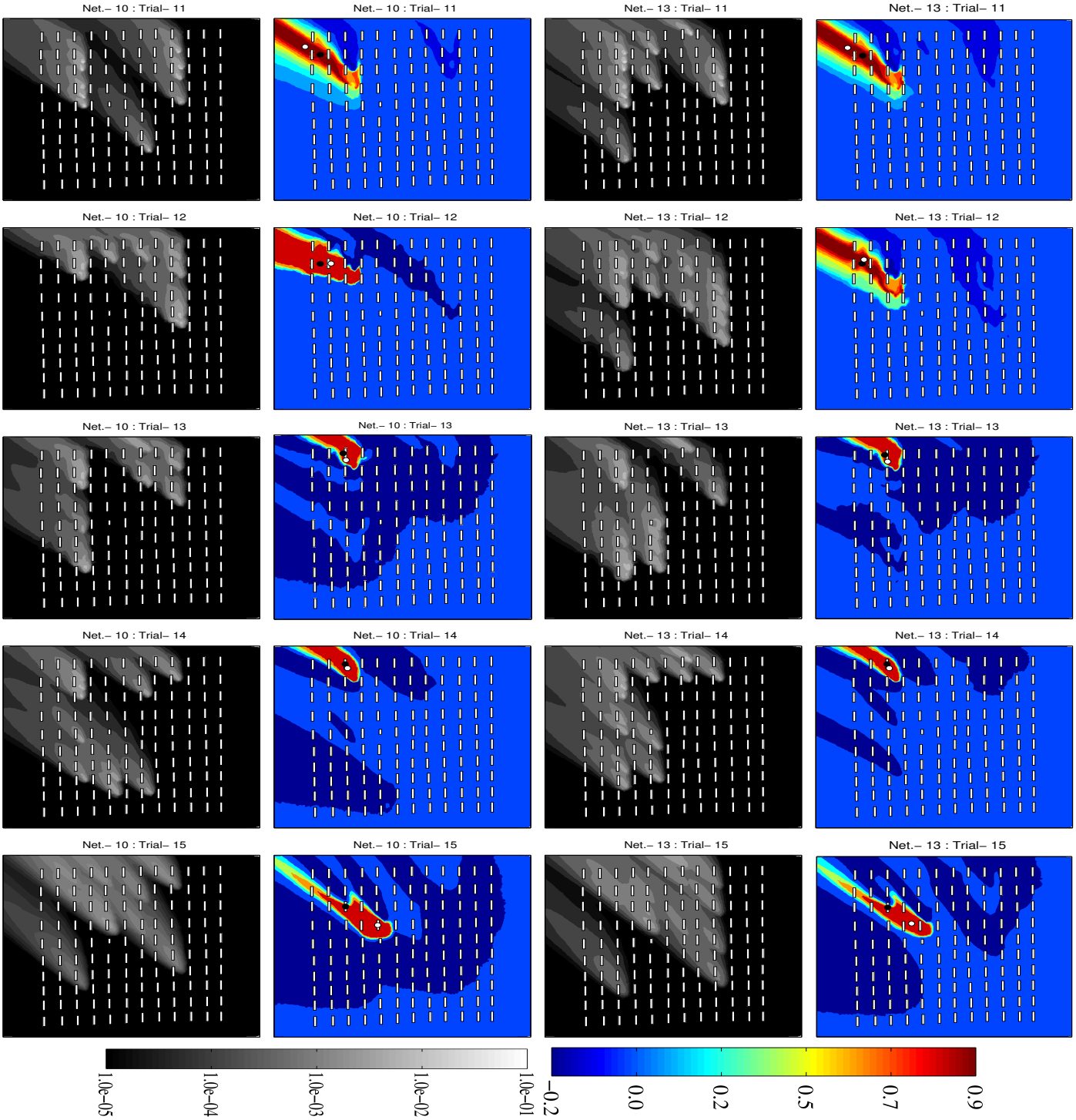

Figure S2.3. Isopleths of the renormalized weight function $(w(\mathbf{x}))$ (gray colored in first and third columns) and the normalized source estimate function $(\mathbf{s}_w^n(\mathbf{x}) = \mathbf{s}_w(\mathbf{x})/\max(\mathbf{s}_w(\mathbf{x})))$ (colored in second and fourth columns) for both optimal network respectively of 10 and 13 sensors for trials 11, 12, 13, 14, & 15. The black and white filled circles respectively represent the true and estimated source locations.

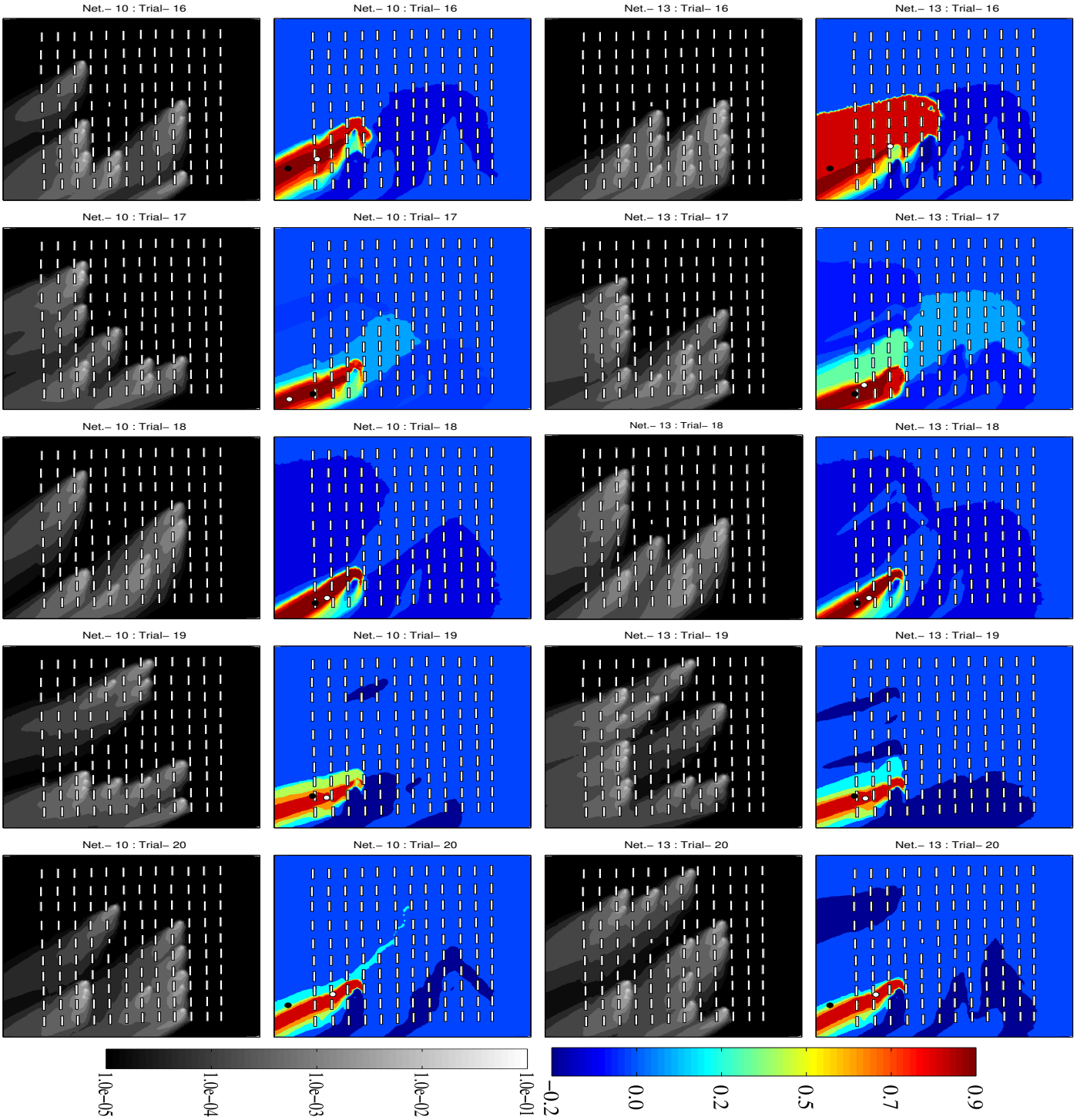

Figure S2.4. Isopleths of the renormalized weight function $(w(\mathbf{x}))$ (gray colored in first and third columns) and the normalized source estimate function $(\mathbf{s}_w^n(\mathbf{x}) = \mathbf{s}_w(\mathbf{x})/\max(\mathbf{s}_w(\mathbf{x})))$ (colored in second and fourth columns) for both optimal network respectively of 10 and 13 sensors for trials 16, 17, 18, 19, & 20. The black and white filled circles respectively represent the true and estimated source locations.

References

Beljaars, A. and Holtslag, A.: Flux parameterization over land surfaces for atmospheric models, Journal of Applied Meteorology, 30, 327–341, https://doi.org/10.1175/1520-0450(1991)030<0327:FPOLSF>2.0.CO;2, http://dx.doi.org/10.1175/1520-0450(1991)030<0327:FPOLSF>2.0.CO;2, 1991.

Ferziger, J. H. and Peric, M.: Computational Methods for Fluid Dynamics, Springer Berlin Heidelberg, https://doi.org/10.1007/978-3-642-56026-2, 2002.

Fluidyn-PANACHE: User Manual, FLUIDYN France / TRANSOFT International, version 4.0.7 edn., 2010.

Gryning, S.-E., Batchvarova, E., Brummer, B., Jorgensen, H., and Larsen, S.: On the extension of the wind profile over homogeneous terrain beyond the surface boundary layer, Boundary-Layer Meteorology, 124, 251–268, https://doi.org/10.1007/s10546-007-9166-9, http://dx.doi.org/10.1007/s10546-007-9166-9, 2007.

Hanjalic, K.: Turbulence And Transport Phenomena: Modelling and Simulation, in: Turbulence Modeling and Simulation (TMS) Workshop, Technische Universität Darmstadt, 2005.

Kumar, P., Feiz, A.-A., Ngae, P., Singh, S. K., and Issartel, J.-P.: CFD simulation of short-range plume dispersion from a point release in an urban like environment, Atmospheric Environment, 122, 645 – 656, https://doi.org/http://dx.doi.org/10.1016/j.atmosenv.2015.10.027, http://www.sciencedirect.com/science/article/pii/S1352231015304465, 2015.

Launder, B.: Turbulence Modelling of Buoyancy-Affected Flows, in: Singapore Turbulence Colloquium, 2004.

Sharan, M. and Kumar, P.: Estimation of upper bounds for the applicability of non-linear similarity functions for non-dimensional wind and temperature profiles in the surface layer in very stable conditions, Proceedings of the Royal Society of London A: Mathematical, Physical and Engineering Sciences, 467, 473–494, https://doi.org/10.1098/rspa.2010.0220, 2010.

Van Doormaal, J. P. and Raithby, G. D.: ENHANCEMENTS OF THE SIMPLE METHOD FOR PREDICTING INCOMPRESSIBLE FLUID FLOWS, Numerical Heat Transfer, 7, 147–163, https://doi.org/10.1080/01495728408961817, http://dx.doi.org/10.1080/01495728408961817, 1984.

Yang, Y., Gu, M., Chen, S., and Jin, X.: New inflow boundary conditions for modelling the neutral equilibrium atmospheric boundary layer in computational wind engineering, Journal of Wind Engineering and Industrial Aerodynamics, 97, 88–95, https://doi.org/http://dx.doi.org/10.1016/j.jweia.2008.12.001, http://www.sciencedirect.com/science/article/pii/S0167610508001815, 2009.